

Traveling waves and worms in ac-driven electroconvection under external multiplicative noise

Jong-Hoon Huh

*Department of Mechanical Information Science and Technology, Faculty of Computer Science and Systems Engineering,
Kyushu Institute of Technology, Fukuoka 820-8502, Japan*

(Received 10 January 2017; published 21 April 2017)

In the presence of external multiplicative noise, ac-driven electroconvection (EC) in a nematic liquid crystal is investigated. Noise-induced traveling waves (TWs) including localized ones (worms) are found with a typical, stationary wave. Three kinds of TWs are classified by their dynamic features (e.g., noise-intensity-dependent Hopf frequency and space-time map). Moreover, ac frequency-dependent threshold voltages of EC are examined in high noise intensities causing abnormal charge redistribution of the EC cell, and the roles of ac and noise fields with respect to TWs are elucidated in successive pattern evolutions. The mechanism of TWs is discussed in terms of a locally perturbed dynamic conductivity due to the noise field additionally applied to the EC; such a conductivity can be related to a weak-electrolyte model for a Hopf bifurcation to a TW.

DOI: [10.1103/PhysRevE.95.042704](https://doi.org/10.1103/PhysRevE.95.042704)

I. INTRODUCTION

Electroconvection (EC) in nematic liquid crystals (NLCs) has been a fascinating physical phenomenon for understanding pattern formations of nonequilibrium systems for the last five decades [1]. The EC system simply consists of a slab of an NLC in an applied electric field. The anisotropy of NLCs provides us with a variety of well-organized EC depending on the amplitude and frequency of the driving ac field, and the symmetry of the (initial) director of the NLCs [1,2]. At a critical voltage V_c , fluctuations in the anisotropic conductivity (due to fluctuations of the director) generate local charge focusing to drive EC from a uniform rest state by a volume force [2]. Generally, one observes stationary, oscillatory, or spatiotemporal chaotic features in EC [3–14]. In the first established theory for EC (one-dimensional Carr-Helfrich mechanism) [15] and the three-dimensionally modified theory [16], the primary instability is well understood with the prediction of the critical voltage V_c and wave vector k_c of the *stationary* rolls (as functions of the driving ac frequency f) [1,2,15–17].

However, the above-mentioned standard model (SM) fails to predict a *traveling* wave (TW) found experimentally as a primary instability; since a TW had first been found in the EC system by Kai and Hirakawa [3], it was intensively discussed by other authors [4–14]. In fact, such an oscillatory instability (TW) was often found as a primary bifurcation in a binary-mixture Rayleigh-Bénard system [18] and in the Taylor-Couette system [19]; however, it always appeared as a secondary bifurcation in the simple-fluid Rayleigh-Bénard system [20]. Fortunately, the TW was successfully understood in the so-called weak-electrolyte model (WEM) taking into account dissociation and recombination of neutral molecules (and also impurities or dopants) in the EC system [8]. In the WEM suggested by Treiber and Kramer, the constant Ohmic conductivity ($\sigma_{\perp}^{\text{eq}}$) was replaced by a dynamical variable: a *local deviation of the conductivity* [$\sigma_{\perp}(\mathbf{r}, t) - \sigma_{\perp}^{\text{eq}}$] from its equilibrium value ($\sigma_{\perp}^{\text{eq}}$) coupling to the director field. The coupling may play a role as a stabilization effect against the primary Carr-Helfrich destabilization effect in the SM. The interplay between such reciprocal effects can generate an oscillatory EC (TW); such an interplay is a common

feature for spontaneous oscillation phenomena (i.e., a Hopf bifurcation) [21]. The additional charge-drift effect against the Carr-Helfrich effect in the WEM is similar to the Soret effect to induce a TW in binary mixtures [18].

More generally speaking, the WEM can be considered as an activator-inhibitor model for a Hopf bifurcation [22]; the essence of the WEM [8] can be simplified in two differential equations:

$$\frac{dA_{\sigma}}{dt} = f(A_{\sigma}, A_n, R), \quad \frac{dA_n}{dt} = g(A_{\sigma}, A_n, R). \quad (1)$$

Here, A_{σ} , A_n , and R denote the amplitude of the local deviation of the conductivity, the director amplitude (i.e., a deviation from the initial director at equilibrium state), and a control parameter (i.e., $R = V^2/V_c^2$), respectively. In the case of $\partial f/\partial A_n < 0$ and $\partial g/\partial A_{\sigma} > 0$ (that can be readily confirmed in the WEM), A_{σ} and A_n play roles as an activator and an inhibitor for a Hopf bifurcation, respectively.

In the WEM, there exist two additional characteristic times, the recombination time τ_{rec} for the relaxation toward the equilibrium state ($\sigma_{\perp}^{\text{eq}}$) and the migration time τ_{mig} (for charges to traverse the cell), as well as two conventional relaxation times for the director (τ_d) and the charge (τ_q) in the SM; typically, $\tau_d \sim O(1 \text{ s})$, $\tau_q \sim O(10^{-2} \text{ s})$, $\tau_{\text{rec}} \sim O(10 \text{ s})$, and $\tau_{\text{mig}} \sim O(10^{-1} \text{ s})$ [8]. Naturally, the SM is recovered for $\tau_{\text{rec}}/\tau_q \rightarrow 0$ (sufficiently fast recombination) and $\tau_{\text{mig}}/\tau_q \rightarrow \infty$ (sufficiently slow drift of the charge) [8]. In addition, it was found that V_c and k_c of the primary EC (as a function of f) differ very little in both models. Therefore, the Hopf frequency f_H of TW ($f_H \neq 0$) is crucial to differentiate both models.

On the other hand, much attention has been paid to the noise impact on EC [23–29]. In particular, noise-induced shift problems in the critical voltage and wave vector of the stationary rolls have been intensively investigated [26–29]. Moreover, it has been discovered that the pattern-formation scenarios are completely changed depending on the characteristic of noise (i.e., its intensity and correlation time) [28,29]. Related to the oscillatory EC (TW), noise may play a role in the pattern transition [e.g., a secondary Hopf bifurcation from a stationary wave (SW, $f_H = 0$) to a TW ($f_H \neq 0$)]. Indeed,

external high-intensity noises induce TWs (TW1 and TW2, see below), and even localized traveling waves (TW3, see below).

In this paper, we focus on noise-induced TWs and their pattern evolutions by varying the ac voltage or the noise intensity. In particular, considering the Hopf frequency of TWs (as functions of the noise intensity and the conductivity), we examine whether the predictions of the WEM are validated in TWs found in this study. Moreover, localized traveling waves (referred to as “worms” in Refs. [10,30]) are investigated under abnormally inhomogeneous conductivity conditions caused by high noise intensity.

II. EXPERIMENT

The standard apparatus for the experimental observation and measurement of EC was used [1,2]; a sinusoidal ac field $E(t) = E_z(t) = \sqrt{2}(V/d) \sin 2\pi ft$ was applied across a thin slab [with a thickness $d = 50 \mu\text{m}$ and a lateral (active) size $L_x \times L_y = 1 \times 1 \text{ cm}^2$] of an NLC [*p*-methoxybenzylidene-*p'*-*n*-butylaniline (MBBA)] sandwiched between two parallel, transparent electrodes (indium tin oxide: ITO). The NLC having conductivity $\sigma_{\perp} = 2.01 \times 10^{-8} \Omega^{-1} \text{ m}^{-1}$ and dielectric constant $\varepsilon_{\perp} = 5.14$ (at $T = 25^\circ\text{C}$ and $f = 120 \text{ Hz}$ of an LCZ meter) was injected in the planar alignment cell [with the initial director $\mathbf{n}_0 = (1, 0, 0)$]; $\sigma_a = \sigma_{\parallel} - \sigma_{\perp} = 6.21 \times 10^{-8} \Omega^{-1} \text{ m}^{-1}$ and $\varepsilon_a = \varepsilon_{\parallel} - \varepsilon_{\perp} = -0.35$ for the present NLC. Here, \parallel and \perp denote the orientations parallel and perpendicular to the initial director \mathbf{n}_0 , respectively. To investigate the role of noise on TWs, a Gaussian-type electric noise $\xi(t)$ was additionally superposed on $E(t)$ ($\xi \parallel E$); it was whitelike noise [with a cutoff frequency $f_c = 100 \text{ kHz}$ and its intensity $V_N = d\sqrt{\langle \xi^2(t) \rangle}$]. EC patterns and their dynamics were observed by using computer-controlled image software (Scion Image) and an image-capture board (Scion Corp., PCI-VE5) via a CCD camera (Sony, XC-75) mounted on a polarizing microscope (Meijitech, ML9300). The details of the experiments were described in our previous papers [28,29].

III. RESULTS AND DISCUSSION

A. Traveling wave and Hopf frequency

Before investigating noise-related TWs, we examined EC in the absence of noise. Two typical EC patterns induced by primary instabilities are presented in Fig. 1. A regular SW [i.e., the so-called Williams domain (WD)] [1–3,31] was found at low frequencies ($f \ll f_{cd} \sim 210 \text{ Hz}$ in the present cell; see below), showing a stationary wave behavior [in the bottom of Fig. 1(a)]. In contrast to the SW, a typical TW appeared at high frequencies near a characteristic frequency f_{cd} (but in the conduction regime: $f < f_{cd}$; see below) [3], as shown in Fig. 1(b); the TW moves to the left-hand side with a constant velocity v along the orientation of the initial director \mathbf{n}_0 ($\|\mathbf{v}\| \parallel \mathbf{k}$). In this case, such a TW accompanies with many defects of the rolls [see those in the central region of the pattern in Fig. 1(b)].

Next, to measure f_H , a space-time map for each TW [e.g., Fig. 2(b)] was obtained by successively placing a one-dimensional image arbitrarily selected in each two-dimensional pattern (e.g., Fig. 1) with an identical time interval (e.g., $\Delta t = 0.1 \text{ s}$ in this study). Then, Fourier transformation

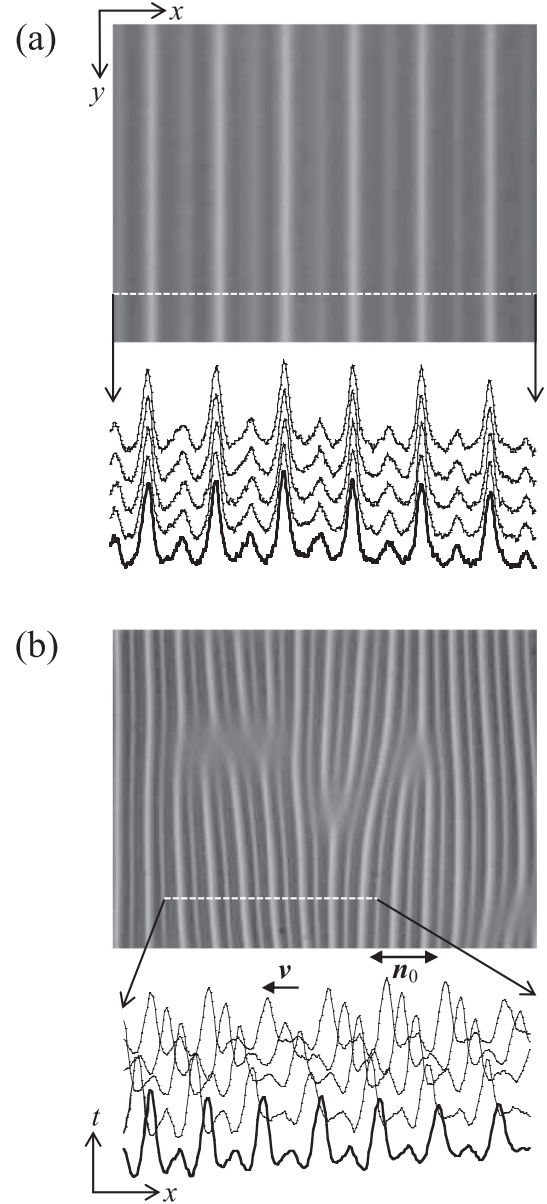


FIG. 1. Typical ac-driven electroconvection patterns in the absence of noise. (a) Stationary wave (SW) at a driving ac frequency $f = 50 \text{ Hz}$ and a reduced ac voltage $\varepsilon = (V^2 - V_c^2)/V_c^2 = 0.1$, (b) Traveling wave (TW) at $f = 200 \text{ Hz}$ and $\varepsilon = 0.1$. To show their dynamics, a one-dimensional light-intensity profile arbitrarily selected in each pattern is presented in the order of time (from $t = 0$ to $t = 4 \text{ s}$). Each frame is $x \times y = 0.421 \times 0.316 \text{ mm}^2$.

of each space-time map was carried out to measure the wave vector k_c and angular frequency ω_c in the power spectrum $S(k, \omega)$ [Fig. 2(c)]. The Hopf frequency f_H was calculated by using $\omega_c = 2\pi f_H = k_c \tan \theta$ [Fig. 2(c)]; it was consistent with the value directly calculated from each space-time map, as shown in Fig. 2(d). Also, the velocity of the TW was measured by using $v = \tan \theta = \omega_c/k_c$ ($\mathbf{v} \parallel \mathbf{k} \parallel \mathbf{n}_0$). In this study, $0 < f_H < 0.5 \text{ Hz}$ and $0 < v < 15 \mu\text{m/s}$ were found in the absence of noise, and $0 < f_H < 1 \text{ Hz}$ and $0 < v < 30 \mu\text{m/s}$ in the presence of noise (see below).

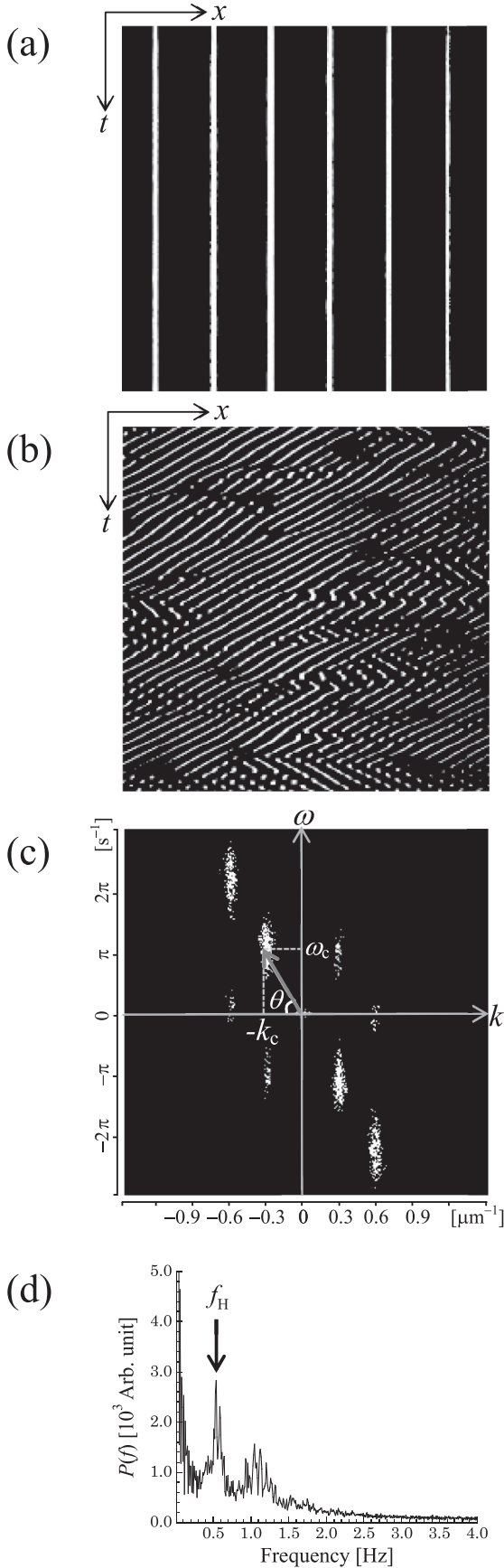


FIG. 2. Typical space-time maps for SW (a) and TW (b), and the power spectrum $S(k, \omega)$ (c) and $P(f)$ (d) for TW (after binary

Usually, the stationary WD (SW) and oscillatory WD (TW) are found without a sudden change in the threshold V_c (as a function of f), as shown in the inset of Fig. 3. Moreover, the wave vector k of the rolls smoothly varies with f (Fig. 3) [8,32]. As mentioned in the Introduction, therefore, the SM cannot distinguish TW from SW in the threshold behavior and wave-vector variation; however, WD and chevron texture (CV) can be classified from the clear difference in $V_c(f)$ and in $k_c(f)$ between below and above f_{cd} [1–3]. Most importantly, one finds a nontrivial, characteristic frequency f_{TW} ($\sim 0.76 f_{cd} \sim 160$ Hz in this study) dividing SW ($f_H = 0$ for $f < f_{TW}$) and TW ($f_H \neq 0$ for $f > f_{TW}$), and the critical dependence of the Hopf frequency f_H on f , as shown in Fig. 3 [4–8,11,12]. Such a frequency f_{TW} can be determined in the WEM, provided many material parameters are completely known for the required conditions [8,12]; it may be calculated as $f_{TW} = f_{TW}(\tau_{rec}, \tau_{mig})$. The behavior of $f_H(f)$ in Fig. 3 (for $\varepsilon_a < 0$) is qualitatively consistent with the earlier results analyzed in the WEM [8,9]. However, the present TWs seem to show a smooth increase of f_H with ac frequency f ; they do not give an abrupt change of slope in $f_H(f)$ for the transition between oblique and normal rolls (i.e., below and above the Lifshitz frequency f_L) observed in the earlier studies for the WEM [8], because they are in the normal-roll regions ($f > f_L$).

B. Three kinds of traveling waves in the presence of noise

We examined f_H of TW as a function of the noise intensity V_N . For both cases ($f < f_{TW}$ and $f > f_{TW}$), f_H was measured with increasing V_N , as shown in Fig. 4; owing to noise, TW appears for $f < f_{TW}$ as well as $f > f_{TW}$. For $f = 50$ Hz ($< f_{TW} \sim 160$ Hz), an ac-driven stable SW (at $V_N = 0$, see Fig. 3) remains, indicating $f_H = 0$ for low V_N (< 18 V), but it undergoes a continuous transition (i.e., a secondary Hopf bifurcation) to TW1 at a critical intensity V_N^* (~ 18 V) and successively develops into TW2, and then into TW3 with increasing V_N . In this evolution, f_H is saturated at a finite value (~ 0.10 Hz) after a smooth increase with V_N . For $f = 170, 200$ Hz ($> f_{TW}$), on the other hand, TW1 appears as a primary instability (at $V_N = 0$; see Fig. 3), and remains with almost V_N -independent f_H (e.g., ~ 0.2 Hz for $f = 200$ Hz) for low V_N (< 19 V); then, it develops into TW2 ($f_H > 0.2$ Hz for $f = 200$ Hz) near $V_N^* \sim 18$ V, and arrives at TW3 (with a saturated $f_H \sim 0.6$ Hz for $f = 200$ Hz) around another critical intensity V_N^\dagger (~ 26 V). The certain critical noise intensities V_N^* and V_N^\dagger evoking or changing TW appear to exist almost without f dependence. In the plateau of f_H (for TW3), the number of worms increases with V_N ($> V_N^\dagger$) [28]; finally, the so-called

FIG. 2. (Continued) image processing). The maps were obtained by placing an arbitrarily selected one-dimensional image (Fig. 1) in time series; each frame is $x \times t = 640$ pixels \times 600 pixels ($= 0.421$ mm \times 60 s). To measure the Hopf frequency $f_H (= \omega_c/2\pi)$ of TW, we define an angle θ ($\tan \theta = \omega_c/k_c$), as shown in (c); the velocity $v (= \tan \theta)$ of TW was calculated by using $2\pi f_H = k_c \tan \theta$. Also, f_H was estimated from the average $P(f)$ of the map (b) for TW.

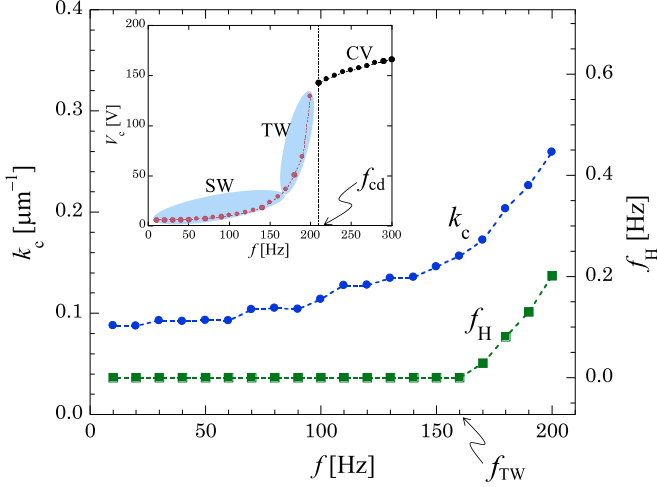


FIG. 3. Threshold voltage V_c , Hopf frequency f_H , and wave vector k_c of Williams domain (WD) as a function of ac frequency f . WD ($f < f_{cd}$) are divided by f_{TW} (~ 160 Hz): SW ($f_H = 0$) for $f < f_{TW}$, and TW ($f_H \neq 0$) for $f > f_{TW}$. Moreover, a typical pattern (chevrons: CV) appears in the dielectric regime ($f > f_{cd}$), which is discriminated from SW and TW in the conduction regime ($f < f_{cd}$) [2].

dynamic scattering mode (DSM) appears [3], where numerous worms combine one another and are totally stirred.

To classify these three kinds of TWs, their space-time maps of light intensity $I(x, t)$ of patterns are demonstrated in Fig. 5. The space-time maps for typical SW, TW1, TW2, and TW3 are shown in Figs. 5(a)–5(d), respectively. In contrast to the regular SW [Fig. 5(a)], TW1 [Fig. 5(b)] is characterized by irregular variations of $I(x, t)$ because of the motion of defects [see also Fig. 1(b)]. However, in contrast to TW1, TW2 [Fig. 5(c)]

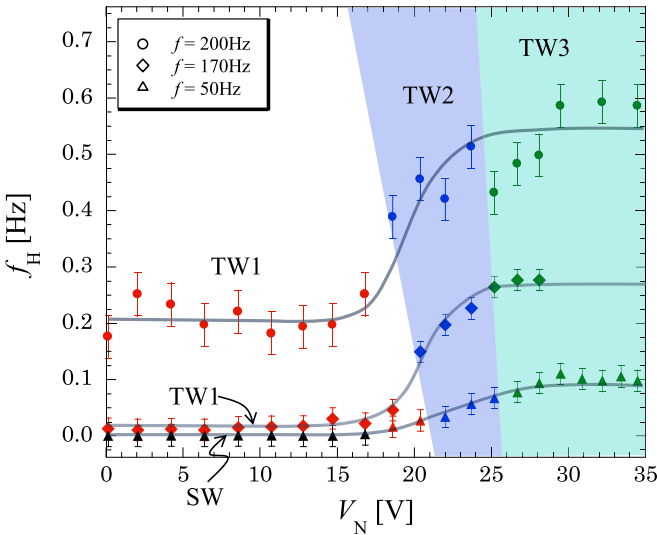


FIG. 4. Dependence of Hopf frequency f_H on the noise intensity V_N . f_H was measured at a fixed $\varepsilon = 0.01$ (near onset). TW1–3 ($f_H \neq 0$) appear for $f = 170, 200$ Hz ($> f_{TW}$), whereas SW ($f_H = 0$) and TW1–3 appear for $f = 50$ Hz ($< f_{TW}$). TW3 is defined as a localized TW (or worms) [see Fig. 8(a)]. The solid lines are a guide for the eye. See also Fig. 5 for SW and TW1–3.

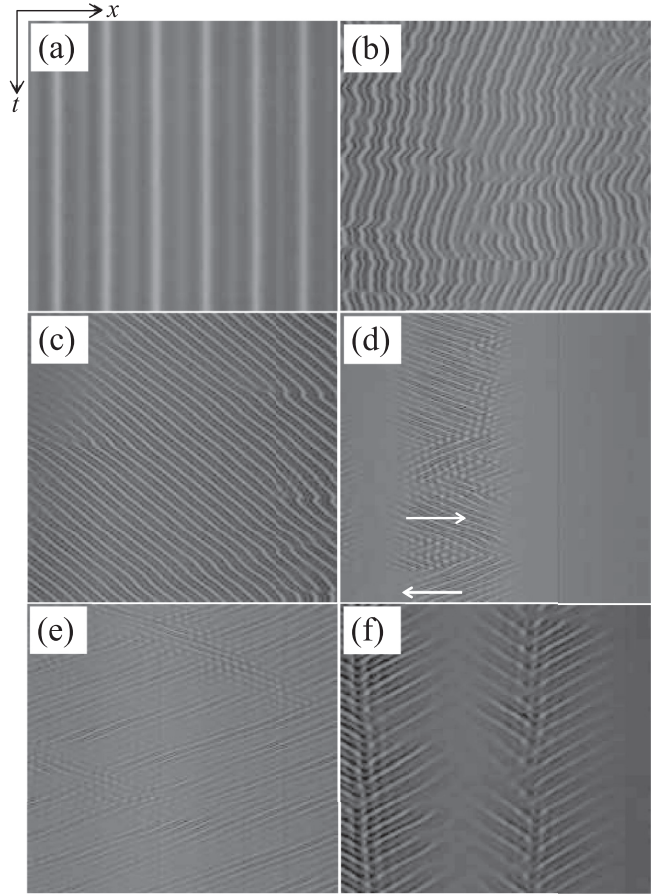


FIG. 5. Typical space-time maps (at a fixed $\varepsilon = 0.05$) for (a) SW ($f = 50$ Hz, $V_N = 5$ V); (b) TW1 ($f = 200$ Hz, $V_N = 10$ V); (c) TW2 ($f = 200$ Hz, $V_N = 20$ V); (d) TW3 ($f = 200$ Hz, $V_N = 30$ V). Moreover, some noticeable TWs were observed: (e) Beating TW2 ($f = 200$ Hz, $V_N = 25$ V) and (f) pair-waves creation and annihilation of TW3 ($f = 170$ Hz, $V_N = 28$ V). The arrows in (d) indicate the traveling direction. Each frame is $x \times t = 640$ pixels \times 600 pixels ($= 0.421$ mm \times 60 s).

does not show such noticeable irregular variations for higher V_N , showing faster velocity (or higher f_H) than that of TW1 (see also Fig. 4). For much higher V_N , inexplicably, TW3 [Fig. 5(d)] appears in a *localized* WD [5,10,30] [see also Fig. 8(a)]. Such a TW3 changes its traveling direction more markedly than other TWs do [see Fig. 5(d)]. Increasing V_N , TW3 (worms) developed into turbulence-based worms (with the colony formation mentioned above [28]); they cannot be classified as such a TW, because they seem to be a kind of DSM rather than TW even though they are localized.

Moreover, an unexpected TW [Fig. 5(e)] showing $I_B(t)$ (like a beat) in Fig. 6 has first been found in the EC system; the period of the beat is $T_{beat} = (10-15)/f_H$ (in this study). Because this TW is frequently found in the V_N region for TW2 (in Fig. 4), it is classified as TW2 in this study. However, this TW with $I_B(t)$ may be distinguished from the typical TW with $I_T(t)$ because of other features beyond the dependence of f_H on V_N (Fig. 4). We may need to consider more than one Hopf mode for understanding the beating TW. A further study is in progress.

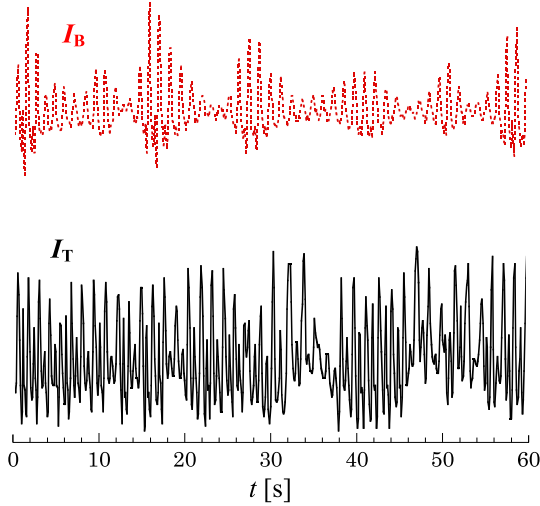


FIG. 6. Light-intensity profiles $I(t)$ obtained (in arb. unit) from an arbitrarily selected temporal line $t(x_0)$ in each space-time map (Fig. 5): $I_B(t)$ for a beating TW from Fig. 5(e) and $I_T(t)$ for a typical TW from Fig. 5(c).

In addition to the TWs, counterpropagating waves in worms were found in Fig. 5(f); they repeatedly arise at both edges of the worms and then disappear at a sink point located in the center of the worms. The pair phase drifts are very similar to those found in localized regions having material parameter ramps [13] or having a laser-induced temperature gradient [33]. This unfamiliar phenomenon is noticeable beyond the details of EC, which can be related to nonlinear phenomena found in many other pattern-formation systems [34,35]; e.g., the pair creation and annihilation of front waves in the Belousov-Zhabotinsky reaction system has often been found [35].

C. Conductivity dependence of Hopf frequency

We tested one of the main predictions of the WEM, $f_H \propto \sigma_{\perp}^{-1/2} d^{-3}$ (at onset) [8,9], in the presence of noise, as shown in Fig. 7. The measured f_H ($f = 200 \text{ Hz} > f_{\text{TW}}$) for TW decreases and becomes zero [i.e., to become SW ($f_H = 0$)] with increasing σ_{\perp} (practically, by increasing temperature T for the NLC cell); although varying T may alter other material parameters, this method has been employed in EC systems [10] under the assumption that T dependence of σ_{\perp} for EC is much stronger than that of others [9]. Around $T = 28^\circ \text{C}$, moreover, no TW is found without any dependence of V_N . This result qualitatively supports the WEM that prefers lower σ_{\perp} (clean) cells for the appearance of TW [8]. Also, the prediction is confirmed in low noise intensities ($V_N = 0, 10 \text{ V}$ for TW1; see also Fig. 4). However, it appears to be inapplicable to a high noise intensity ($V_N = 25 \text{ V}$ for TW2; see also Fig. 4). In addition, TW3 (worms for $V_N > V_N^{\dagger} \sim 26 \text{ V}$ in Fig. 4) seems also to be outside of the WEM (not seen in Fig. 7). It is because TW1 ($f > f_{\text{TW}}$) arises as a primary instability predicted in the WEM, but TW2 and TW3 occur as secondary instabilities by high noise intensity beyond the WEM.

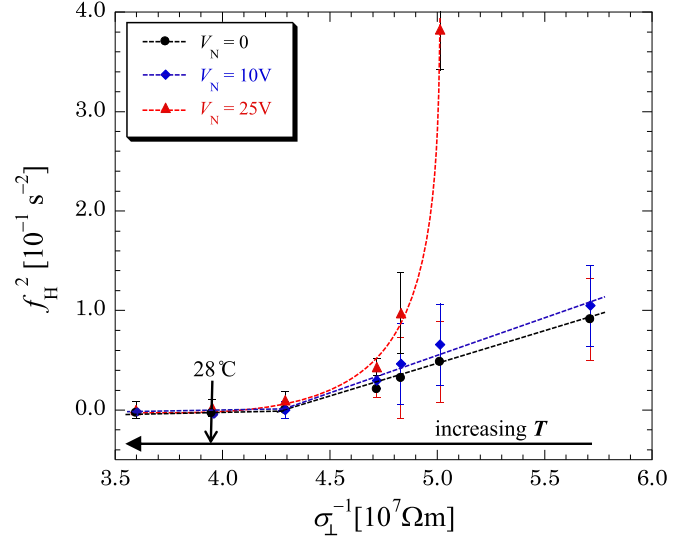


FIG. 7. Dependence of Hopf frequency f_H on the conductivity σ_{\perp} (at a fixed $\varepsilon = 0.01$ and $f = 200 \text{ Hz}$). The relation $f_H \propto \sigma_{\perp}^{-1/2} d^{-3}$ predicted in the WEM is confirmed for $V_N = 0, 10 \text{ V}$ (TW1), whereas it is inapplicable to $V_N = 25 \text{ V}$ (TW2). The frequency f_H (and velocity v) of TWs decreases (i.e., to become slower TW) and then becomes zero [i.e., SW ($f_H = 0$)] with increasing σ_{\perp} (i.e., with increasing temperature T); $\sigma_{\perp} = \sigma_{\parallel} \sim 5.66 \times 10^{-8} \Omega^{-1} \text{ m}^{-1}$ at the nematic-isotropic transition temperature $T_c \sim 40^\circ \text{C}$ for the NLC.

Considering the dependence of σ_{\perp} on f_H [8] and also on V_c [2,32], we checked the threshold voltage $V_c(f)$ for EC in localized worm regions and their surrounding regions [see the two selected regions in Fig. 8(a)]. While the noise ($V_N = 30 \text{ V} > V_N^{\dagger}$) was applied to EC [which was able to induce worms (TW3) with the required conditions of the ac field], the respective functions $V_c(f)$ were measured for the two regions, as shown in Fig. 8(c). Obviously, two kinds of $V_c(f)$ appear in a single cell, which are similar to that in Fig. 3 (including TW); this reflects that the conductivities in the two regions differ from each other (as known in the SM) [2]. In the case of $f > f_{\text{cd}} \sim 160 \text{ Hz}$ (for the surrounding region of worms), therefore, CV (typical EC for the dielectric regime: $f > f_{\text{cd}}$) simultaneously arises with worms (EC for the conduction regime $f < f_{\text{cd}}$) in a single cell [Fig. 8(b)]. From the behavior of two kinds of $V_c(f)$ [in particular, f_{cd} (worm region) $> f_{\text{cd}}$ (no worm region)], one can presume that the worm region has larger conductivity than the no worm region does [2,32]; f_{cd} (worm region) $\sim 220 \text{ Hz}$ estimated in the SM ($f_{\text{cd}} = (2\pi\tau_q)^{-1}[\zeta^2(\sigma_{\perp}/\sigma_{\parallel}) - 1]^{1/2}$) [2].

These results tell us that noise-redistributed charges are much more plentiful in worm regions than those in no worm regions. Moreover, it was found that this charge inhomogeneity shows a hysteresis; both regions remain distinguishable [through $V_c(f)$] on the order of hours after removing the applied noise ($V_N \rightarrow 0$). No TW3 (traveling worms) was found after $V_N \rightarrow 0$ (and $V \neq 0$), but highly developed turbulence in the localized region remains at high V ; the region may be yielded by noise-induced thermal focusing [29]. It is worthwhile to mention that such worms can arise either from inhomogeneity in critical material parameters [13,33] or from spatially localized solutions in the relevant Ginzburg-

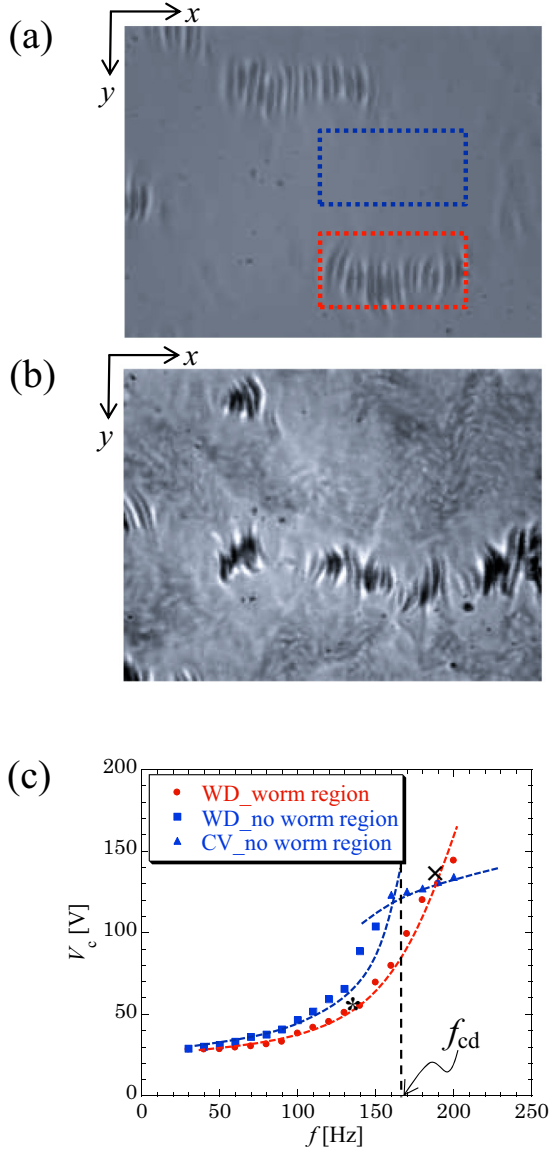


FIG. 8. Different threshold functions $V_c(f)$ for EC in the two regions (in the presence of noise $V_N = 30$ V). (a) TW3 (worms) and two selected regions (dotted rectangular places); (b) coexistence of chevrons (CV) and TW3 ($f = 180$ Hz); (c) threshold voltages $V_c(f)$ for the two regions. The patterns (a,b) were observed at the points symbolized as * and x in (c), respectively. Each frame for (a) and (b) is $x \times y = 0.421 \times 0.316$ mm².

Landau equations even in homogeneous media [36]; our study supports at least the former case. Also, the importance of the dependence of conductivity on worms had been pointed out in earlier studies: for $\sigma_a < 0$ [37] or for $\sigma_a > 0$ [10] (and this study).

Moreover, although they do not appear in such extremely inhomogeneous charge redistribution for worms (TW3), TW1 and TW2 may be induced by locally perturbed conductivity (due to the external noise); we need to note that this is a crucial point in the WEM (i.e., a local deviation of the conductivity from its equilibrium value) [8]. In other words, noise may reinforce the deviation of the conductivity with the WEM; this noise effect gives rise to the unique pattern

evolutions: TW1 \rightarrow TW2 \rightarrow TW3 ($f > f_{TW}$) and SW \rightarrow TW1 \rightarrow TW2 \rightarrow TW3 ($f < f_{TW}$) [Fig. 4]. It can be said that at least the slow TW1 (with low f_H) for low $V_N (< V_N^*)$ can be understood in the WEM (Figs. 4 and 7). However, the fast traveling or beating TW2 (with high f_H), and the localized TW3 (worms) (and its behavior such as the pair creation and annihilation of the waves) still remain outside of the WEM as well as the SM.

D. Roles of ac and noise fields

To elucidate the roles of ac and noise fields for TW, we examined pattern evolutions with increasing V or V_N . In Figs. 9(a)–9(d), a pattern evolution [from SW ($f = 30$ Hz $< f_{TW}$)] with increasing V ($V_N = 0$) is shown using space-time maps. Moreover, as a reduced ac voltage $\varepsilon [(V^2 - V_c^2)/V_c^2 = 0.01]$ is fixed, a pattern evolution is given in the same way with increasing V_N [Figs. 9(e)–9(h)]. Continuously increasing V , a regular SW destabilizes and develops into defect chaos [Fig. 9(b)] [3]; the number (and also velocity) of the defects increases with V [Figs. 9(b)–9(d)]. Despite much higher V , no TW is found [Figs. 9(c) and 9(d)]; instead, developed turbulence (i.e., DSM) is found [3]. On the other hand, the noise field induces a TW [Fig. 9(f)] from an SW [Fig. 9(e)]. In addition, the higher V_N is applied, the faster TW (with higher f_H) is observed [Figs. 9(f)–9(h)].

Furthermore, by increasing V (i.e., ε), we checked a pattern evolution from a TW ($f = 200$ Hz $> f_{TW}$) at a fixed noise intensity ($V_N = 25$ V). A beating TW2 [showing $I_B(t)$ in Fig. 6] [Fig. 10(a)] found at $\varepsilon = 0.10$ degrades into a typical TW1 [Fig. 10(b)] at $\varepsilon = 0.45$, and then changes into defect chaos [Fig. 10(c)] at $\varepsilon = 0.50$. Increasing V much higher ($\varepsilon = 0.90$), a pattern showing fast, periodic motions of defects is found [Fig. 10(d)]; similarly to Fig. 9(d) [10], it does not travel ($f_H = 0$) but it is completely different from the regular SW [Figs. 9(a) and 9(e)]. To evaluate this pattern evolution more clearly, f_H was measured as a function of ε in the presence of noise with different intensities ($V_N = 0, 10, 25$ V). In Fig. 11, TW2 ($V_N = 25$ V) and TW1 ($V_N = 0, 10$ V) change into the pattern ($f_H = 0$) [Fig. 10(d)] with increasing ε . It is obvious that the ac field weakens or even removes the Hopf mode (i.e., the deviation of the equilibrium conductivity). This result is similar to that in binary mixtures; as large Rayleigh-number-induced convective flows homogenize the fluid [18], large ε -induced EC may remove the conductivity-deviation effect for TW.

From these results, it can be said that the roles of ac and noise fields are quite different from each other for the pattern formation including TW. The ac field is not crucial to induce TW (i.e., a Hopf bifurcation), even though a TW appears near f_{cd} in the absence of noise [3]; it plays a role as a reducer (or even as a remover) of TW for its sufficiently high intensity [Figs. 10 and 11]. In contrast to the ac field, the noise field generates TW and fosters faster and more complicated TW, and even localized TW (worms) for its sufficiently high intensity (i.e., locally perturbed conductivity due to the random oscillation of charges by noise). Moreover, the noise can induce a transition from SW (or even defect chaos and a highly turbulent state) to TW. Accordingly, we can speculate that competition between ac and noise effects to TWs determines

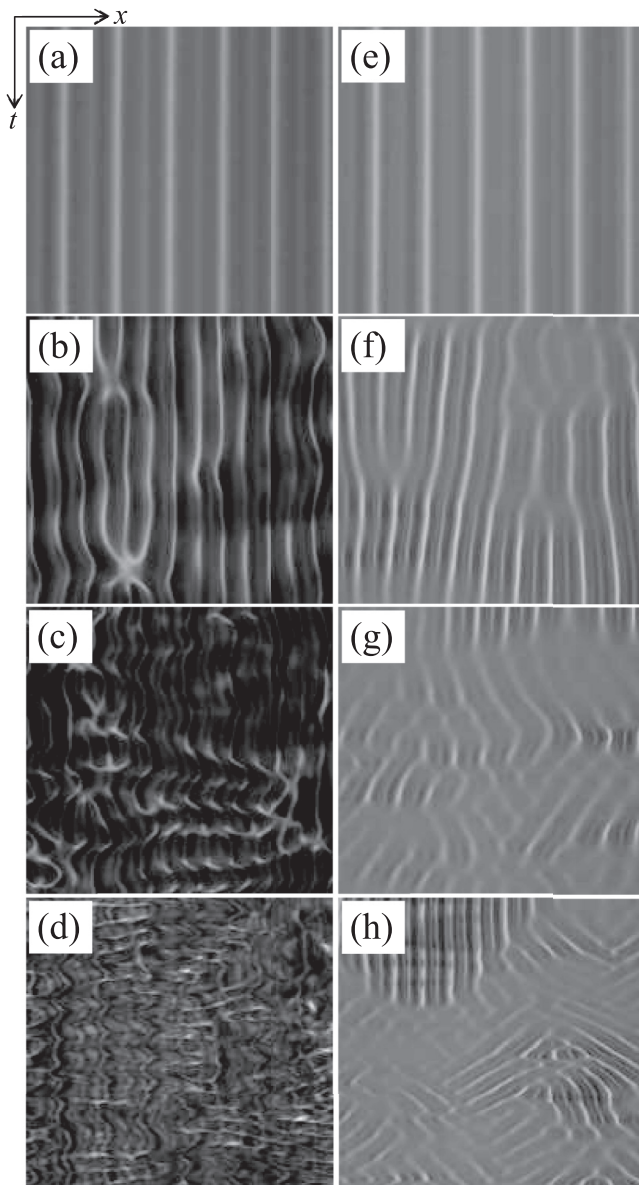


FIG. 9. Space-time maps ($f = 30 \text{ Hz} < f_{\text{TW}}$) with increasing the ac voltage V [(a–d) at $V_N = 0$], and with increasing the noise intensity V_N [(e–h) at $\varepsilon = 0.01$]: $V = 6.35 \text{ V}$ (a), 7.44 V (b), 8.68 V (c), 9.92 V (d), and $V_N = 12.2 \text{ V}$ (e), 19.5 V (f), 21.8 V (g), 27.0 V (h). Increasing V gives rise to defect chaos (b), whereas increasing V_N induces TW (f) which develops into the faster TW (TW1 \rightarrow TW2). Each frame is $x \times t = 640 \text{ pixels} \times 600 \text{ pixels}$ ($= 0.421 \text{ mm} \times 60 \text{ s}$).

the patterns and their evolution scenarios. In other words, a noise-induced (or -reinforced) tendency toward TW (N_{eff}) and an ac-developed motion of defects against TW (A_{eff}) gives (i) SW, defect chaos, or DSM for $A_{\text{eff}} > N_{\text{eff}}$; (ii) TW1–3 for $A_{\text{eff}} \sim N_{\text{eff}}$; and (iii) noise-dominated patterns or DSM for $A_{\text{eff}} < N_{\text{eff}}$ [29]. Namely, the Hopf bifurcation (TW) arises in two comparable, reciprocal effects. In one-dimensional EC cells without motion of defects, a critical investigation on these evolution scenarios is now in progress.

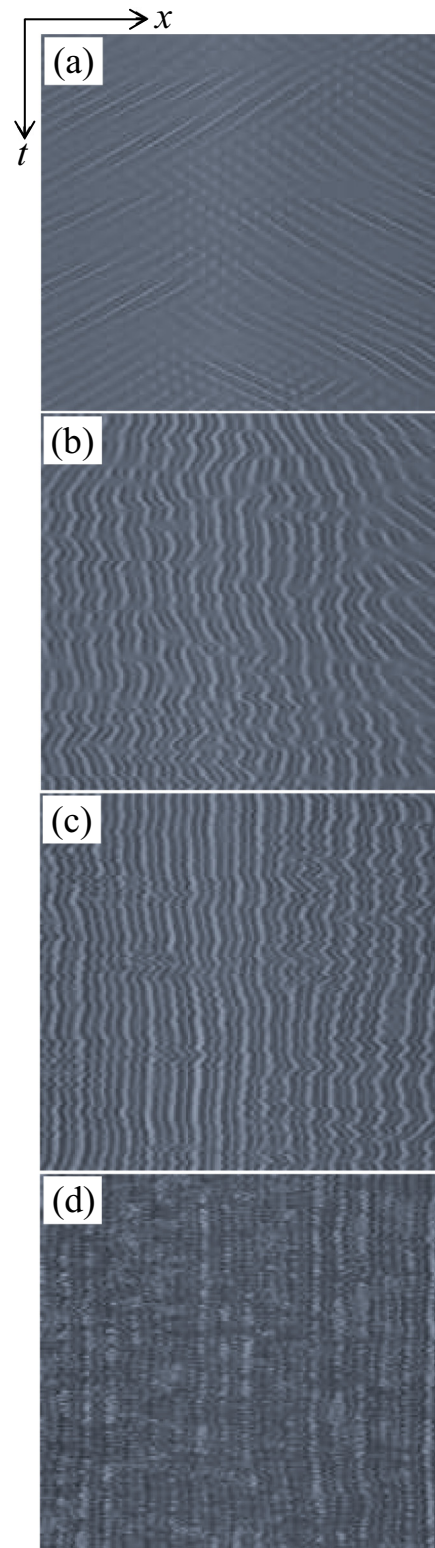


FIG. 10. Space-time maps ($f = 200 \text{ Hz} > f_{\text{TW}}$) with increasing the ac voltage V (i.e., ε) (at a fixed $V_N = 25 \text{ V}$): $\varepsilon = 0.10$ (a), 0.45 (b), 0.50 (c), 0.90 (d). When increasing V , TW2 (a) degrades into TW1 (b), and then changes into defect chaos (c,d). No TW is found in high ac voltages. Each frame is $x \times t = 640 \text{ pixels} \times 600 \text{ pixels}$ ($= 0.421 \text{ mm} \times 60 \text{ s}$).

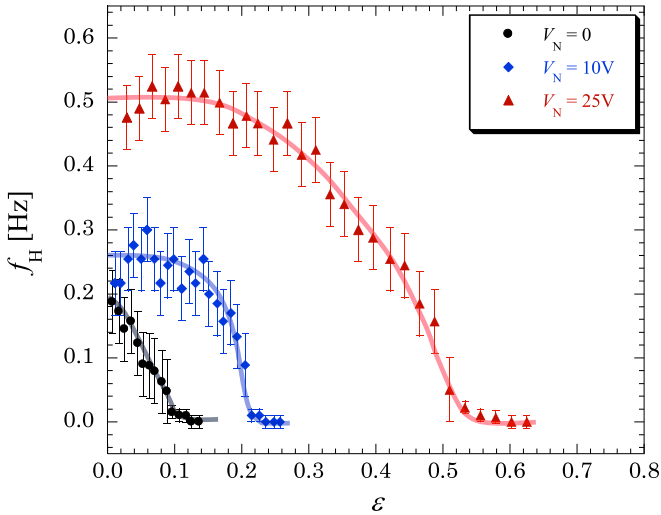


FIG. 11. Dependence of Hopf frequency f_H on a reduced ac voltage ε ($f = 200$ Hz) in the absence ($V_N = 0$) and presence ($V_N = 10, 25$ V) of noise. TW2 ($V_N = 25$ V) and TW1 ($V_N = 0, 10$ V) change into completely different EC not traveling ($f_H = 0$) with increasing ε . The solid lines are a guide for the eye. See also Fig. 10.

On the other hand, for low noise intensities ($V_N < V_N^* \sim 18$ V in this study), the noise does not play such a role for TW (see Fig. 4). In this range of V_N , the noise only suppresses the Carr-Helfrich instability (i.e., completely different stabilization effect) so that the critical voltage V_c monotonically increases with V_N (i.e., $V_c^2 = V_0^2 + bV_N^2$, $b > 0$ for white noise; here, V_0 and b denote a threshold voltage for WD at $V_N = 0$ and a response sensitivity of WD to noise, respectively) [28,29]; it is not enough to induce the dynamical conductivity deviation for TW.

IV. SUMMARY AND CONCLUSIONS

In the ac-driven electroconvection (EC) system, traveling waves (TWs) and localized waves (worms) have been investigated in the presence of external multiplicative noise. Depending on the ac frequency f and the noise intensity V_N ,

three kinds of TWs have been found; they could have been characterized by their space-time maps. Moreover, the Hopf frequency of TWs has been discussed in the weak-electrolyte model (WEM) that was suggested for understanding a Hopf bifurcation to a TW in the EC system [8]. The crucial point of the WEM, a local deviation of the conductivity (i.e., dynamical charge redistribution), has been validated in the experimental results obtained in this study. However, some noise-reinforced TWs such as a beating TW and a localized TW appear to be outside of the WEM. Unexpectedly, the present TWs are found for $f < f_{TW}$ as well as for $f > f_{TW}$; notice that the TW in the WEM can arise as a primary instability only for $f > f_{TW}$, a critical frequency for a Hopf bifurcation. In addition, the roles of ac and noise fields have been demonstrated in pattern evolutions including TWs; the ac field plays a role as a reducer or a remover of TW, whereas the noise field induces a TW and develops it into faster and complicated ones. In high noise intensities ($V_N > V_N^* \sim 26$ V) generating extremely inhomogeneous charge redistribution, worms (a kind of TW) arise being independent of f .

As the drifting local charges are induced by the weak electrolyte (and couple to the director-amplitude mode for TW) in the WEM, noise can generate the drift of local charges for the appearance of TWs. When such a stabilization effect due to the charge drift against the destabilization effect (i.e., the primary Carr-Helfrich instability) oscillates by their mutual feedback of the two effects, the system gives rise to a Hopf bifurcation to a TW [36,38]. More generally speaking, the charge-drift mode and the director-amplitude mode correspond to an activator and an inhibitor in a well-known general model for a Hopf bifurcation, respectively [22]. However, the detailed features of TWs found in this study still remain as open problems. Recently, noise-induced oscillations and noise-induced frequency shifts have become an attractive area of research for understanding pattern formations in nonequilibrium systems, and also for exploiting the time-dependent nature and environment [39–41]. This study will give a useful hint to the recent studies.

ACKNOWLEDGMENTS

We thank T. Nagaya and Y. Hidaka for critical reading of the manuscript and helpful comments. This study was supported by JSPS KAKENHI (Grant No. 15K05215).

[1] See reviews and references herein: e.g., T. John, J. Heuer, and R. Stannarius, *Phys. Rev. E* **71**, 056307 (2005); A. Buka, N. Eber, W. Pesch, and L. Kramer, *Phys. Rep.* **448**, 115 (2007).
 [2] L. M. Blinov, *Electro-optical and Magneto-optical Properties of Liquid Crystals* (The Universities Press (Belfast) Ltd., Northern Ireland, 1983).
 [3] S. Kai and K. Hirakawa, *Prog. Theor. Phys. Suppl.* **64**, 212 (1978).
 [4] R. Ribotta, A. Joets, and L. Lei, *Phys. Rev. Lett.* **56**, 1595 (1986).
 [5] A. Joets and R. Ribotta, *Phys. Rev. Lett.* **60**, 2164 (1988).
 [6] I. Rehberg, S. Rasenat, J. Fineberg, M. de la Torre Juárez, and V. Steinberg, *Phys. Rev. Lett.* **61**, 2449 (1988).

[7] I. Rehberg, S. Rasenat, and V. Steinberg, *Phys. Rev. Lett.* **62**, 756 (1989).
 [8] M. Treiber and L. Kramer, *Mol. Cryst. Liq. Cryst.* **261**, 311 (1995); M. Dennin, M. Treiber, L. Kramer, G. Ahlers, and D. S. Cannell, *Phys. Rev. Lett.* **76**, 319 (1996); M. Treiber and L. Kramer, *Phys. Rev. E* **58**, 1973 (1998).
 [9] M. Treiber, N. Éber, Á. Buka, and L. Kramer, *J. Phys. II France* **7**, 649 (1997).
 [10] M. Dennin, G. Ahlers, and D. S. Cannell, *Science* **272**, 388 (1996); *Phys. Rev. Lett.* **77**, 2475 (1996); M. Dennin, D. S. Cannell, and G. Ahlers, *Phys. Rev. E* **57**, 638 (1998); N. Éber, P. Salamon, B. A. Fekete, R. Karapinar, A. Krekhov, and A. Buka, *ibid.* **93**, 042701 (2016).

- [11] S.-Q. Zhou, N. Éber, Á. Buka, W. Pesch, and G. Ahlers, *Phys. Rev. E* **74**, 046211 (2006); S.-Q. Zhou and G. Ahlers, *ibid.* **74**, 046212 (2006).
- [12] T. Tóth-Katona, A. Cauquil-Vergnes, N. Éber, and Á. Buka, *Phys. Rev. E* **75**, 066210 (2007).
- [13] K. K. Vardanyan and D. R. Spiegel, *Phys. Rev. E* **76**, 031703 (2007).
- [14] G. Acharya, G. Dangelmayr, J. Gleeson, and I. Oprea, *Int. J. Mol. Sci.* **12**, 4488 (2011).
- [15] E. F. Carr, *Mol. Cryst. Liq. Cryst.* **7**, 253 (1969); W. Helfrich, *J. Chem. Phys.* **51**, 4092 (1969).
- [16] E. Bodenschatz, W. Zimmermann, and L. Kramer, *J. Phys. (Paris)* **49**, 1875 (1988); L. Kramer, E. Bodenschatz, W. Pesch, W. Thom, and W. Zimmermann, *Liq. Cryst.* **5**, 699 (1989).
- [17] J.-H. Huh, Y. Hidaka, and S. Kai, *Mol. Cryst. Liq. Cryst.* **366**, 833 (2001).
- [18] H. Brand and V. Steinberg, *Physica A* **119**, 327 (1983); *Phys. Lett. A* **93**, 333 (1983); D. T. J. Hurle and E. Jakeman, *J. Fluid Mech.* **47**, 667 (1971); R. W. Walden, P. Kolodner, A. Passner, and C. M. Surko, *Phys. Rev. Lett.* **55**, 496 (1985).
- [19] C. D. Andereck, S. S. Liu, and H. L. Swinney, *J. Fluid. Mech.* **164**, 155 (1986).
- [20] F. H. Busse, *J. Fluid Mech.* **52**, 97 (1992).
- [21] H. G. Rotstein and R. Kuske, *Physica D* **215**, 46 (2006); B. Echebarria and A. Karma, *Phys. Rev. E* **76**, 051911 (2007).
- [22] D. Kaplan and L. Glass, *Understanding Nonlinear Dynamics* (Springer-Verlag, New York, 1995); R. C. Desai and R. Kapral, *Dynamics of Self-Organized and Self-Assembled Structures* (Cambridge University Press, Cambridge, 2009).
- [23] W. Horsthemke and R. Lefever, *Noise-Induced Transitions* (Springer-Verlag, Berlin, 1984).
- [24] J. Garcia-Ojalvo and J. M. Sancho, *Noise in Spatially Extended Systems* (Springer-Verlag, New York, 1999).
- [25] F. Sagués, J. M. Sancho, and J. García-Ojalvo, *Rev. Mod. Phys.* **79**, 829 (2007).
- [26] S. Kai, T. Kai, M. Takata, and K. Hirakawa, *J. Phys. Soc. Jpn. Lett.* **47**, 1379 (1979); H. Brand and A. Schenzle, *J. Phys. Soc. Jpn.* **48**, 1382 (1980); S. Kai, H. Fukunaga, and H. Brand, *J. Phys. Soc. Jpn. Lett.* **56**, 3759 (1987).
- [27] T. Kawakubo, A. Yanagita, and S. Kabashima, *J. Phys. Soc. Jpn.* **50**, 1451 (1981).
- [28] J.-H. Huh, A. Kuribayashi, and S. Kai, *Phys. Rev. E* **80**, 066304 (2009); J.-H. Huh and S. Kai, *J. Phys. Soc. Jpn. Lett.* **78**, 043601 (2009); **83**, 063601 (2014).
- [29] J.-H. Huh, *J. Phys. Soc. Jpn. Lett.* **76**, 033001 (2007); **79**, 123602 (2010); *Phys. Rev. E* **84**, 025302(R) (2011); **92**, 062504 (2015); *J. Phys. Soc. Jpn.* **85**, 024002 (2016); *Phys. Rev. E* **94**, 052702 (2016).
- [30] Y. Tu, *Phys. Rev. E* **56**, R3765(R) (1997); H. Riecke and G. D. Granzow, *Phys. Rev. Lett.* **81**, 333 (1998).
- [31] R. Williams, *J. Chem. Phys.* **39**, 384 (1963).
- [32] J.-H. Huh, Y. Hidaka, A. G. Rossberg, and S. Kai, *Phys. Rev. E* **61**, 2769 (2000).
- [33] N. C. Giebink, E. R. Johnson, S. R. Saucedo, E. W. Miles, K. K. Vardanyan, D. R. Spiegel, and C. C. Allen, *Phys. Rev. E* **69**, 066303 (2004); D. R. Spiegel, E. R. Johnson, and S. R. Saucedo, *ibid.* **73**, 036317 (2006).
- [34] T. Nagaya, H. Hotta, H. Orihara, and Y. Ishibashi, *J. Phys. Soc. Jpn.* **60**, 1572 (1991); A. V. Ilyenkov, L. V. Kreminskaya, M. S. Soskin, and M. V. Vasnetsov, *J. Nonlinear Opt. Phys. Mater.* **6**, 169 (1997); R. R. Guimaraes, R. S. Mendes, P. R. G. Fernandes, and H. Mukai, *J. Phys.: Condens. Matter* **25**, 404203 (2013).
- [35] S. C. Muller, O. Steinberg, and J. Schutze, *Physica A* **188**, 47 (1992).
- [36] A. V. Gaponov-Grekhov and M. I. Rabinovich, *Nonlinearities in Action* (Springer-Verlag, Berlin, 1992).
- [37] H. R. Brand, C. Fradin, P. L. Finn, W. Pesch, and P. E. Cladis, *Phys. Lett. A* **235**, 508 (1997).
- [38] M. Cross and H. Greenside, *Pattern Formation and Dynamics in Nonequilibrium systems* (Cambridge University Press, Cambridge, 2009).
- [39] L. Yang, Z. Hou, and H. Xin, *J. Chem. Phys.* **110**, 3591 (1999).
- [40] L. Ridolfi, P. D'Odorico, and F. Laio, *Noise-Induced Phenomena in the Environmental Sciences* (Cambridge University Press, Cambridge, UK, 2011).
- [41] D. S. A. Simakov and J. Pérez-Mercader, *Sci. Rep.* **3**, 2404 (2013).